Research Article

Influence of sodium-based activators and water content on the fresh and hardened properties of metakaolin geopolymers

Isabel Pol Segura[1] (ID) · Peter Arendt Jensen[1] · Anne Juul Damø[1] · Navid Ranjbar[2] · Lars Skaarup Jensen[3] · Mariana Canut[3]

© The Author(s) 2022   OPEN

Abstract
Several studies explore optimal molar oxide ratios for metakaolin geopolymer production. However, there is not a consensus on the optimal mix, and within similar range large differences in compressive strength are reported, and consequently in the overall performance. Hence, the present work selects a specific molar oxide ratio that leads to strengths above 30 MPa (SiO_2/Al_2O_3 ratio of 3.19, a Na_2O/Al_2O_3 of 1.00, and a water-to-solids ratio of 0.52), and investigates the individual effect of the sodium-based activators (NaOH and Na_2SiO_3) and the water content on fresh and hardened properties of metakaolin geopolymers. The tested properties include the rheology, setting time, mass loss, shrinkage, density and compressive strength. The test results show that an increase of water content (water-to-solids > 0.52) and increase of NaOH (Na_2O/Al_2O_3 > 1.03) have the largest impact, showing a detrimental effect on both fresh and hardened properties. Moreover, the best results are obtained when using molar ratios of SiO_2/Al_2O_3 at 3.14, Na_2O/Al_2O_3 at 0.97 and a water-to-solids ratio of 0.51, which is within the range of optimum molar ratios from previous studies. The tests are further supplemented by Thermogravimetric analysis/Differential scanning calorimetry (TGA/DSC), scanning electron microscopy (SEM), and X-ray diffraction (XRD).

Article highlights

- An elevated water content can improve the fluidity of the pastes, however, it increases pore formation and detriments the strength.
- A surplus of alkali content decreases the fluidity, accelerates the setting, and increases the shrinkage and surface cracking of metakaolin geopolymers.
- The best performance is achieved with a water-to-solids = 0.51, and molar oxide ratios of $Na_2O/Al_2O_3 = 0.97$ and $SiO_2/Al_2O_3 = 3.14$.

✉ Isabel Pol Segura, isapol@kt.dtu.dk | [1]Department of Chemical and Biochemical Engineering, Technical University of Denmark, 2800 Kgs. Lyngby, Denmark. [2]Department of Mechanical Engineering, Technical University of Denmark, 2800 Kgs. Lyngby, Denmark. [3]Department of Research and Development, FLSmidth, 2500 Valby, Denmark.

1 Introduction

Portland cement is the binder of concrete and has an approximate annual production of 4 billion tonnes with a 4% growth per annum [1, 2]. The main concern is that an average of 0.6 tonnes of CO_2 are released per tonne of cement produced [3]. Thus, this makes the cement industry one of the major contributors to the global anthropogenic CO_2 emissions, being its share 8% in 2020 [4–6].

Several actions such as energy efficiency, alternative binders or fuels and carbon capture have been proposed with the ultimate goal of decarbonizing the cement production [7]. One of the promising low-CO_2 alternatives are geopolymer binders [8, 9]. Geopolymers are synthesized by the reaction of an aluminosilicate-based material and alkali activators under the presence of water [10]. They form an amorphous three-dimensional aluminosilicate structure by the combination of $[SiO_4]^{4-}$ and $[AlO_4]^{5-}$ tetrahedra. The incorporation of alkalis, such as Na^+ or K^+, balance the electrical charges of the network [10, 11]. This reaction leads to a geopolymer paste that can set and harden at room temperature, and can gain mechanical properties over time [12].

Common aluminosilicate-based materials include industrial wastes such as coal fly ash and blast furnace slags from the coal and steel industry respectively, or pre-treated natural sources such as metakaolin [12–14]. Meanwhile, the most used alkali activators are generally a combination of NaOH and Na_2SiO_3, as they are relatively cheaper option than other alkalis [15, 16]. Moreover, they can increase the cohesion of the network, lower the porosity and enhance their overall durability against carbonation and chemical attacks [17].

Significant research has been dedicated over the last decades to investigate the influence of the mix design on the mechanical properties of geopolymers [18], with special attention to high-calcium precursors such as fly ash [19–21] and slags [22–24]. In comparison, a lower number of studies have been dedicated to low-calcium precursors such as metakaolin or other calcined clays as they tend to require higher water demand and exhibit lower workability [25]. Nevertheless, there is a growing interest on optimizing the properties of calcined clay/metakaolin-based geopolymers due to raw materials availability [25, 26], and literature reports 28-day strengths between 20 to 80 MPa with molar oxide ratios in the ranges of SiO_2/Al_2O_3 of 2.5–4, Na_2O/Al_2O_3 of 0.6–1.2, and H_2O/Al_2O_3 of 10–11 [27–33]. In addition, besides similar work conducted by Albidah [34] and Alghannam [35] in metakaolin based concrete, to the authors' best knowledge there is still a lack of studies comparing the rheology of the fresh metakaolin geopolymer pastes with their hardening evolution properties, microstructure and resulting mechanical strength.

Thus, in this study the focus is to explore the relationship between metakaolin's geopolymer properties and the different alkali activator concentrations (NaOH and Na_2SiO_3), and water contents. The objective is to have a better understanding of how individually each reagent affects several of the fresh and hardened metakaolin geopolymer properties, so that they can then be optimized to achieve the best performance. The tested properties are: rheology, setting time, compressive strength, density, mass loss, shrinkage, and thermal stability. Moreover, the results are supplemented by studying microstructure and mineralogical composition.

In the next section, the materials and methods are described (Sect. 2). In Sect. 3, the results of the study are presented together with the discussion, and in Sect. 4, the conclusions summarize the main findings and underline the importance of this research.

2 Materials and methods

Geopolymer pastes were synthesized by mixing metakaolin with an alkaline solution constituted by sodium hydroxide and sodium silicate. Metakaolin (MetaMax) was supplied by BASF Chemicals (Ludwigshafen, Germany) with a surface area of 13.49 m^2/g and a mean particle size of 4.56 μm. The chemical oxide composition measured by X-ray Fluorescence (XRF) is given in Table 1. SiO2 and Al2O3 are the main components, with contents of 53.0 wt% and 43.8 wt%, respectively.

Sodium hydroxide (NaOH) solution was obtained by dissolving NaOH pellets from Sigma Aldrich (98% purity) in distilled water. Sodium silicate (Na_2SiO_3) solution was purchased from Honeywell with a composition of 14.7% Na_2O, 29.4% SiO_2 and 55.9% H_2O (SiO_2/Na_2O molar ratio of 2); and a specific gravity of 1.4 g/cm^3 at 20 °C.

The alkaline solution was prepared for 4 min by mixing the NaOH solution into the Na_2SiO_3 solution. Due to the exothermic reaction taking place, the alkaline solution was prepared 4 h in advance to be allowed to cool down to room temperature. Thereafter, the metakaolin powder was added into the alkaline solution and mixed for 4 min in a mechanical Hobart mixer. Once a homogenous mixture was obtained, the properties of the geopolymer paste were ready to be tested.

Table 1 Chemical oxide composition of BASF metakaolin

SiO2	Al2O3	Na2O	K2O	TiO2	Fe2O3	CaO	MgO	P2O5	SO3	LOI
53.0%	43.8%	0.23%	0.19%	1.70%	0.43%	0.02%	0.03%	0.03%	0.03%	0.46%

In this study, 13 different geopolymer formulations were prepared and the mix design variables are shown in Table 2. As it can be seen, there is a reference geopolymer mixture (REF) which serves as our starting point, and the molar oxide ratios have been selected based on prior studies that reported compressive strengths above 30 MPa [27]. Thereafter, the mixes have been arranged in four groups and one reagent has been varied in each of them. Group W, varies the content of distilled water, group SH the content of sodium hydroxide, group SSS the amount of sodium silicate solution and SSW maintains constant the water-to-solids ratio while varying the solid sodium silicate content, as it was observed that in group SSS there was a combined effect of two different variables (water and solid sodium silicate content). Something else that can be observed is that water-to-solids ratio below 0.5 was not possible to achieve in this study due to the poor workability observed on the pastes. Other studies have reported water-to-solids below 0.45, however, they also had lower SiO_2/Al_2O_3 (around 2.5) or had added superplasticizers [34, 36].

Thereafter, several fresh and hardened properties have been tested for each specimen to investigate the effect of the alkaline reagent concentration and water-to-solids ratio. The fresh properties measured were rheology and setting time. For testing the rheological properties; shear strain, shear stress, shear rate, storage modulus, loss modulus and viscosity; of the different pastes were studied using an Anton Paar Physica MCR 502 rheometer equipped with a parallel plate system with a 25 mm diameter. A pre-shearing at high shear was done before measurements to bring all samples to a similar fluidity level. Meanwhile, the setting time was tested using an automatic Vicat apparatus with continuous penetration at ambient conditions (E044-03N), following the EN196-3 standard [37].

The hardened properties tested over time were mass loss, shrinkage, density and compressive strength. The fresh homogenous mixtures were casted into 40 mm cubes and placed for 30 s on a vibration table to remove any trapped air bubbles. The samples were then inserted in a curing chamber at 21 °C ± 2 °C and 80% relative humidity (RH). They were unmoulded after 24 h and they were left in the curing chamber until testing. The mass loss, shrinkage, and density were measured after 1, 3, 7, 14, 21, 28 and 56 days. The shrinkage was determined by measuring the change in length of 40 mm cubes using a micrometer with 0.01 mm accuracy. The weight of each cube was recorded before each length measurement. The density (ρ) was then back-calculated, knowing the volume (V) of the sample and the weight (m), $\rho = \frac{m}{V}$.

Compressive strength tests were performed on the cubic samples using a Digitec E160-01D compression machine with a constant loading rate of 0.750 MPa/s. Tests were performed after 3, 7 and 28 days. Each reported value corresponds to the average of three measurements.

The samples were further characterized by thermogravimetric analysis/differential scanning calorimetry (TGA/DSC), scanning electron microscopy (SEM), and X-ray diffraction (XRD). The wet geopolymer pastes were casted in 10 mm cubes, vibrated for 30 s and placed in the curing chamber (21 °C ± 2 °C and 80% RH) until testing. The samples had to be powdered in a ball mill at 350 rpm for 3 min before testing them on TGA–DSC and XRD, while hardened dry cubes were used in SEM–EDS. TGA/DSC was used to measure the thermal stability and phase change of the different formulations at 7 and 28 days. The analyses

Table 2 Mix proportions and molar oxide ratios of metakaolin geopolymer pastes

	Exp	Metakaolin (g)	Na$_2$SiO$_3$ solution (g)	NaOH pellet (g)	Water (g)	Na$_2$O/Al$_2$O$_3$ (mol/mol)	SiO$_2$/Al$_2$O$_3$ (mol/mol)	H$_2$O/Al$_2$O$_3$ (mol/mol)	Water/ solids (g/g)
	REF	400	400	60	105	1.00	3.19	10.62	0.52
Group W	W1	400	400	60	110	1.00	3.19	10.79	0.52
	W2	400	400	60	120	1.00	3.19	11.11	0.54
	W3	400	400	60	150	1.00	3.19	12.08	0.59
Group SH	SH1	400	400	85	105	1.18	3.19	10.62	0.50
	SH2	400	400	65	105	1.03	3.19	10.62	0.51
	SH3	400	400	45	105	0.89	3.19	10.62	0.53
Group SSS	SSS1	400	380	60	105	0.97	3.14	10.26	0.51
	SSS2	400	410	60	105	1.01	3.22	10.80	0.52
	SSS3	400	440	60	105	1.05	3.31	11.35	0.54
Group SSW	SSW1	400	380	60	110	0.97	3.14	10.42	0.51
	SSW2	400	410	60	100	1.01	3.22	10.64	0.51
	SSW3	400	440	60	91	1.05	3.31	10.89	0.51

were performed using a Netzsch STA 449 in the temperature range between 0 and 1100 °C, with a heating rate of 10 °C/min, and with an atmosphere of 10% O_2 and 90% N_2. The morphological microstructure was studied on the specimens after 28 days by SEM–EDS. A Thermo Scientific Prisma E with a 20 kV acceleration voltage was used. The samples were non-polished to study the morphology with secondary electron images. Finally, the mineralogical and phase composition of the metakaolin and the geopolymers were investigated at 28 days by using a Huber G670 diffractometer with CuKα (λ = 0.154 nm). The scans were performed within the range of 2θ = 10–100° at 40 kV and scanning times of 5 h.

3 Results and discussions

3.1 Rheological properties

Strain sweep measurements have been carried out to determine the linear viscoelastic domain and the main critical strain values of the samples. The critical strain is associated with the breakage of early reaction products [38], and it's obtained at the end of the linear elastic regime of the geopolymers. Figure 1 presents the evolution of the storage modulus (G') and the loss modulus (G'') as a function of the shear strain. Only one sample of each group has

been selected, as the critical shear strain value was found to be almost the same for all mixtures. The different samples were subjected to a pre-shearing with an oscillation frequency of 1 Hz and a shear strain range from 0.001 to 100%. The critical strain was observed at 0.01. Thereafter, to ensure that any structural build-up has been removed and the samples are brought to a reference level, the taken critical strain for the following rheological measurements is in the order of 10 times the critical strain (0.1).

Moreover, Fig. 1 also shows the shear strain at which the storage (G') and the loss modulus (G'') become equal. This indicates a change in behaviour of the material from solid ($G' > G''$) to liquid ($G' < G''$) due to the increased shearing applied. It can be seen that the shear strain at which the $G' = G''$, is the same in almost all samples (~ 0.3).

Figure 2 presents the shear flows measured at 25 °C for two sample mixes of each group. Group W shows in Fig. 2a) that even at a slight increase of water content (W1, W3) with respect to REF geopolymer, the shear stress decreases. This is probably due to the higher fluidity of those pastes, which results in a lower resistance to shearing [39]. Thereafter, in Fig. 2b) it can be seen that the increase of NaOH (SH1) leads to a higher shear stress than REF. It has to be noted that in SH1 the water-to-solids ratio is also lower with respect to REF, so the combination of those two factors are hindering the fluidity of this paste [39, 40]. Groups SSS and SSW shown
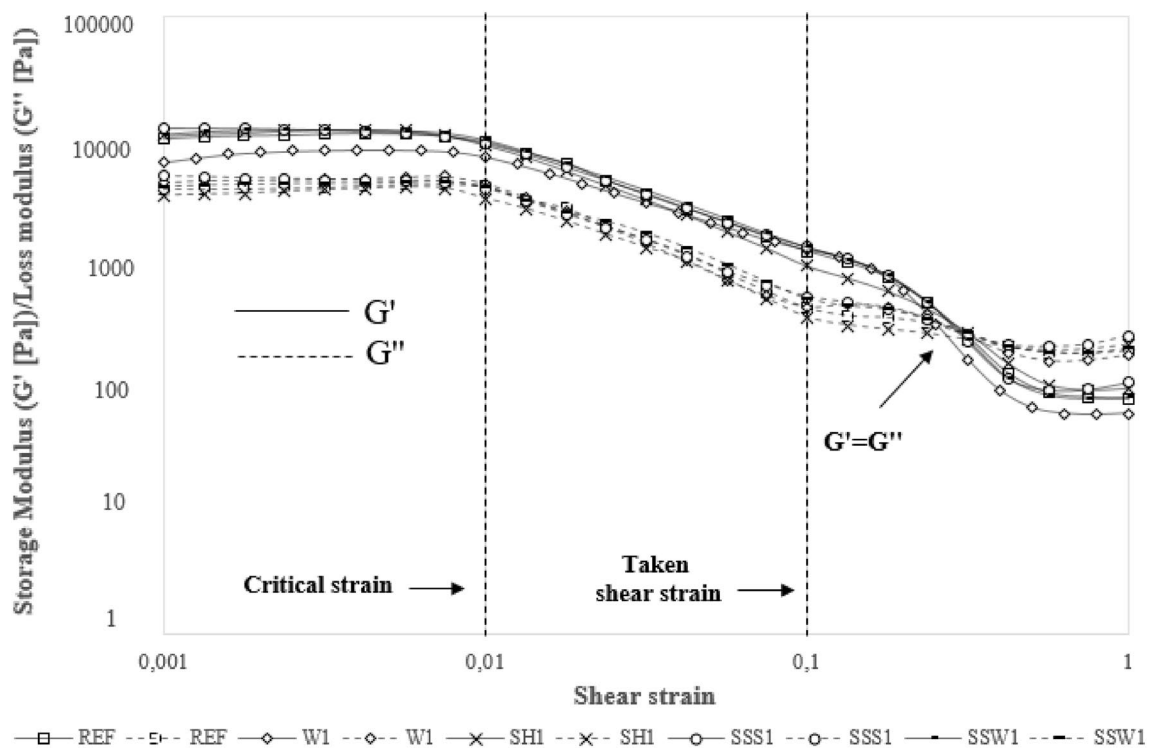

Fig. 1 Storage modulus/loss modulus vs shear strain for REF, W1, SH1, SSS1 and SSW1
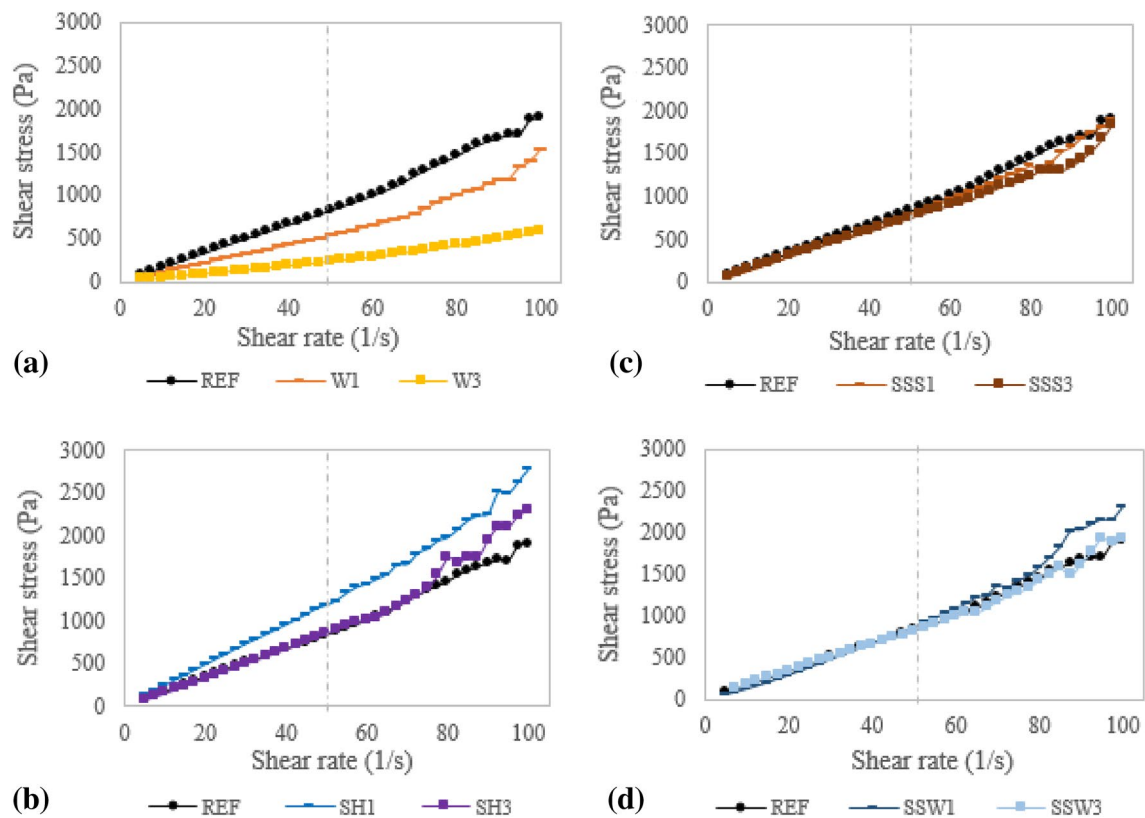
Fig. 2 Shear stress vs shear rate of the different group formulations at 25 °C being **a** group W, **b** group SH, **c** group SSS, and **d** group SSW

respectively in Fig. 2c and d, present similar resistance to gradual deformation as for the REF sample. Generally, it has been observed that soluble silica tends to increase the shear stress on geopolymer systems, however with a lower degree than soluble NaOH [39, 40]. Conversely, an increased water content reduces the shear stress. Thus, it seems as there is a counter-balance effect from those two parameters in those pastes, resulting in a similar resistance to deformation to the REF paste.

It can also be seen that the shear stress is directly proportional to the shear rate, especially up to a shear rate of 50 s^{-1}, this means that it can be considered as a special case of the Bingham equation (Eq. 1) in which $\tau_O = 0$. This means that even though geopolymers have been identified as non-Newtonian, they can be assumed to have a behavior of a Newtonian fluid with a constant plastic viscosity [40–42].

$$\tau = \tau_o + \mu\dot{\gamma} \qquad (1)$$

where: τ is the shear stress (Pa), μ is plastic viscosity and $\dot{\gamma}$ is the shear strain rate (s^{-1}) [42].

For Newtonian fluids, the viscosity of the fluid is the coefficient of proportionality between the shear stress and the shear rate [41]. Thereafter, the slopes of the linear relationships found in Fig. 2 (up to shear rate of 50 s^{-1}), are the Newtonian viscosities of the studied specimens and they are presented in Table 3.

Correspondingly to the shear stress flow observations, it can be seen that when comparing to the REF sample, the largest impact on the viscosities is given by an increase of water or NaOH content [39, 40]. The lowest viscosity is found for W3 (4.46 Pa s^{-1}), which has the highest water-to-solids ratio (0.59), and is within range of typical values found for the intrinsic viscosity of Portland cement pastes

Table 3 Viscosity of the tested metakaolin geopolymers at 25 °C and 1 Hz

Geopolymer	Viscosity (Pa s^{-1})
REF	16.59
W1	10.70
W3	4.46
SH1	23.96
SH3	16.56
SSS1	15.54
SSS3	14.89
SSW1	16.51
SSW3	16.45

(4 to 6 Pa s^{-1}), depending on their composition [43–45]. Meanwhile, the highest viscosity has been found to be the one with the highest sodium hydroxide content (SH1) and lowest water-to-solids ratio. This can be mainly due to the higher viscosity of the NaOH solution, when compared to water, and also due to an increased concentration of Na$^+$ ions which increases the rate of rigidification as a higher dissolution of metakaolin occurs [46]. Sodium silicate solution is also a purely viscous fluid [47], and as seen from group SSS and SSSW, it increases the overall viscosity of metakaolin geopolymer pastes (15–17 Pa s^{-1}), when compared to Portland cement pastes. From a rheological point of view, metakaolin geopolymer pastes tend to have a higher viscosity than Portland cement pastes, and they are greatly affected by the viscosity of the alkali activator solution [26]. This higher viscosity tends to hinder the workability of the fresh pastes. In addition, it has been suggested that metakaolin geopolymer pastes in contrast of a Portland cement paste, does not behave as a granular suspension since its viscosity is mostly controlled by the interstitial fluid and not by the direct frictional contact of metakaolin grains [46, 47].

3.2 Setting times

The initial and final setting times are measured to investigate the effect of the different mix designs on the stiffening of the paste. This is important as the initial setting indicates the time that the paste starts to lose its plasticity, while the final setting, the time that the paste has completely stiffen and can sustain some load. This means that the initial set, provides the time frame that the geopolymer paste is workable and that can be casted/shaped. The EN 196-3 [37] prescribes that the initial setting time of a cement paste should not be earlier than 45 min and the final setting should not be later than 600 min. Figure 3 presents the setting times obtained for the different geopolymer pastes. At a first glance it can be observed that all samples comply within the standards.

Thereafter, Group W shows that the higher the water-to-solids ratio (W3), the slower the initial and final setting time. This is due to the fact that higher water-to-solid ratio implies a higher water concentration in the alkali solution, which reduces the rate of geopolymerization reaction and dissolution of metakaolin [48]. Subsequently, Group SH indicates that the higher the NaOH concentration and higher molar ratio Na$_2$O/Al$_2$O$_3$ (SH1), the faster the setting times. This is caused by the fact that high NaOH concentration accelerates the rate of geopolymerization and the dissolution of silica and alumina, which causes a faster setting [49]. In group SSS, it is observed that the higher content of sodium silicate solution (SSS3), the slower the setting time. However, in this group the effect is divided between the increase of water-to-solids ratio and the solid content of sodium silicate. Hence, in group SSW, the water-to-solids ratio is kept constant while only the solid sodium silicate is varied. Similarly to group SSS, increasing the solid sodium silicate (SSW3) leads to slower setting times. According to previous literature [50, 51], higher SiO$_2$/Al$_2$O$_3$ molar ratio, leads to longer setting times due to an increased amount of soluble silica in the solution. The presence of a high amount of soluble silica makes the geopolymerization reaction take more time to complete the early stage reaction, resulting in an increase of setting time. Moreover, when comparing the setting times from Fig. 3 with the fresh paste viscosities of Table 3, it seems as the pastes with higher viscosity tend also to faster setting times. This is probably related with the relative higher content of NaOH in those samples, thus resulting in an acceleration of the geopolymerization rate [47].
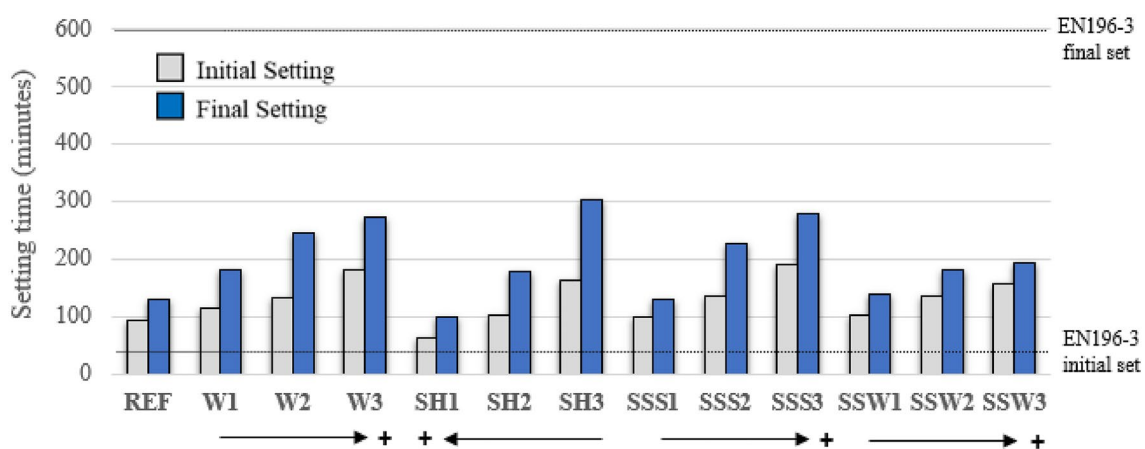

Fig. 3 Initial and final setting time of the different metakaolin geopolymer formulations. The (+) and (→) indicate the gradual reagent increase of each group

3.3 Shrinkage, mass loss and density

The shrinkage, mass loss and density of the synthesized metakaolin geopolymers were tested over a period of 56 days for all specimens. The measured mass loss and uniaxial length change of the different pastes are presented in Fig. 4. It can be seen from the figure that the mass loss and length change are more pronounced in the first 21 days of curing. Geopolymer mixes REF and SH2 showed the least amount of mass loss after 56 days (− 1.16% and − 1.19%, respectively), while geopolymer mix W3 displayed clearly the highest amount of mass loss (− 2.15%). This mass loss is mainly associated in the literature with free water evaporated from macropores [52], and consequently it is observed that the mass loss is increased, at higher water-to-solids ratio. Regarding the shrinkage of the pastes, geopolymer mix SH1, W3 and SSS3 showed the highest length change at 56 days (− 1.01%, − 0.98% and − 0.94%, respectively). This indicates that the shrinkage of the pastes is not only influenced by the free water evaporated from macropores (drying shrinkage), but also from an increased alkalinity of the solution. The increase of Na^+ ions might be leading to finer pore sizes (mesopores) [53], and structural water evaporation from mesopores can then generate capillary stresses that induce autogenous shrinkage [52].

Figure 5a–d compares the mass loss of the pastes with their corresponding total shrinkage. The total shrinkage has been calculated as the multiplication of the average uniaxial length change of the cube paste times two. From this figure, it can be confirmed that as a general trend the higher the mass loss, the higher the total shrinkage. As mentioned before, this is mainly due to the loss of free water from the macropores of the geopolymer pastes that leads to a loss in weight, and predominantly corresponds to drying shrinkage, which seems to have the largest effect on the metakaolin geopolymer pastes. However, it can also be directly observed that SH1 has the highest shrinkage without having the highest mass loss, as this shrinkage might be induced by internal capillary stresses generated from the higher alkalinity (autogenous shrinkage). Those results are in agreement with previous observations [54, 55] which indicated that the volume change of metakaolin geopolymer pastes is mainly due to drying shrinkage rather than autogenous shrinkage. Moreover, the shrinkage (%) values obtained in this study are within the range of previously reported shrinkages, however, greater mass loss in the order of 10 to 30% has been previously reported when curing the metakaolin geopolymers at ambient conditions [55]. In addition, it has to be noted that the low shrinkage values observed in metakaolin geopolymers when compared to Portland cement pastes, have also been previously explained by an early age expansion related to the formation of aluminium phases [56, 57].

Thereafter, the density was measured over a period of 56 days for each specimen (Table 4). It is observed that the density results slightly vary among the different compositions, having lower densities (lighter materials) the ones that have a higher water-to-solids ratio and highest sodium silicate content. The density of geopolymers tends to modestly decrease with age of curing as a result of free water evaporation, and it is in agreement with the corresponding mass loss and drying shrinkage. The average metakaolin geopolymer density at 56 days has been found to be 1.8 g/cm^3, and is within the range of densities that have been previously reported for metakaolin geopolymers varying from 1.6 to 2 g/cm^3 depending on the alkalinity of the solution [58]. Comparing the average
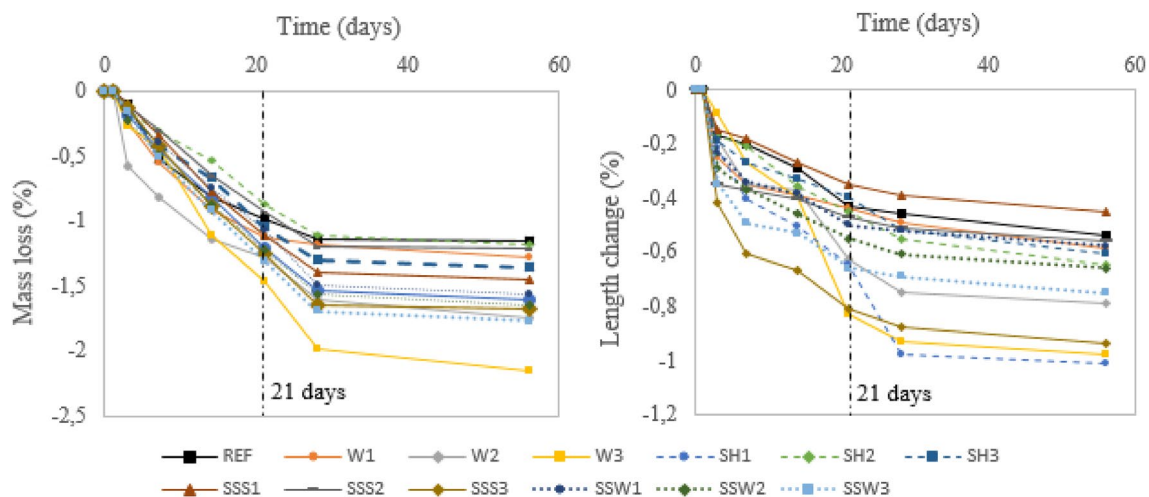

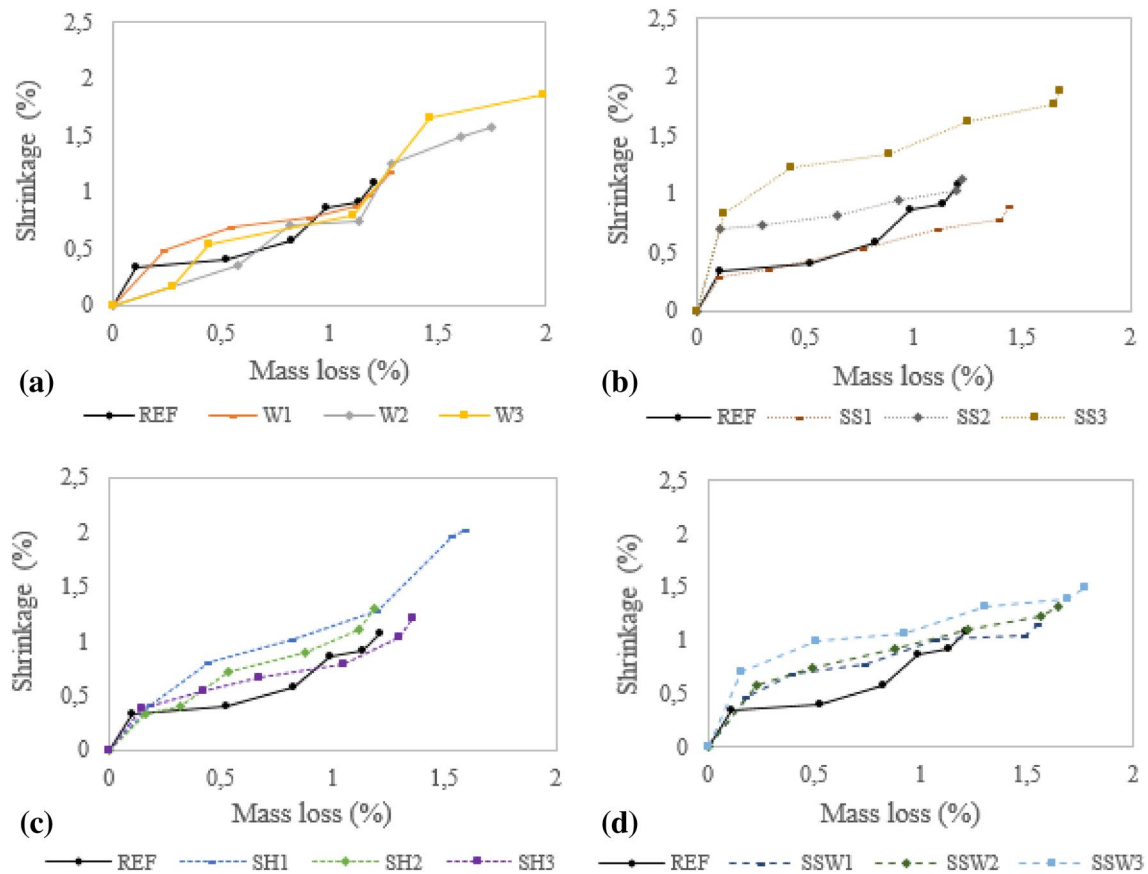**Fig. 4** Mass loss (%) and length change (%) for a period of 56 days

Fig. 5 Comparison of the mass loss and drying shrinkage (%) from **a** group W, **b** group SH, **c** group SSS, and **d** group SSW

Table 4 Measured density (g/cm³) at 56 days of curing

REF	W1	W2	W3	SH1	SH2	SH3	SSS1	SSS2	SSS3	SSW1	SSW2	SSW3
1.81	1.79	1.76	1.74	1.83	1.81	1.75	1.82	1.79	1.78	1.81	1.77	1.75

metakaolin geopolymer density after 56 days (1.8 g/cm³) with a typical Portland cement paste (2.3 g/cm³), it can be seen that the metakaolin pastes have a lower density [59]. This is in agreement with the reported specific gravity ratio of metakaolin geopolymers which is 2.3, while for Portland cement is 3.15 [60], and it can also be correlated to the lower-packing density and higher specific surface area of metakaolin when compared to Portland cement [61, 62].

3.4 Compressive strength

Compressive strength development for the geopolymer formulations tested at 3, 7 and 28 days are shown in Fig. 6. Standard deviation of the three measured samples has also been included. From the figure it is seen that at 7 days, all the specimens have gained the 80–90% of the compressive strength obtained at 28 days. This agrees with the fact that metakaolin enhances the early strength development

and accelerates the initial setting time when compared to fly ash or slag geopolymers [63, 64].

Figure 6a shows that the mix W3 with highest water-to-solids ratio ($w/s = 0.59$) leads to the lowest compressive strength (23.8 MPa) after 28 days, and that all specimens in group W (with increased water content compared to REF sample) lead to lower compressive strengths than REF geopolymer. This correlates with prior observations [34], which observed a decrease in compressive strength when increasing the water-to-solids ratio from 0.4 to 0.54.

Meanwhile, Fig. 6b illustrates the effect of the sodium hydroxide concentration, in which it can be seen that the highest concentration of NaOH (SH1) can lead to an early strength similar to the one obtained with REF, however, there is a limited strength gain after 7 days. This is probably due to a surplus of Na^+ ions, and instead of being incorporated in the geopolymer matrix, they stayed free weakening the overall microstructure [65]. Previous work
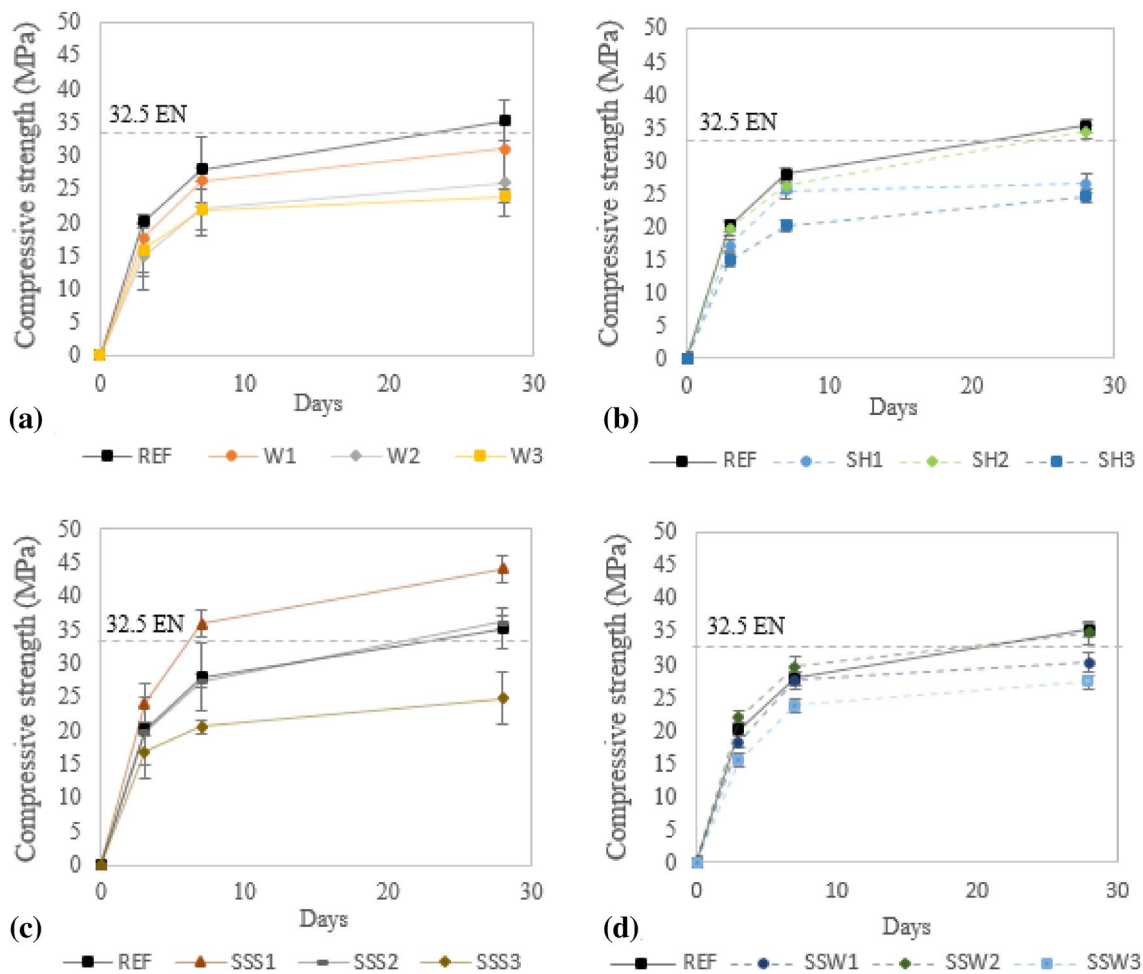
Fig. 6 Compressive strength development over time of **a** group W, **b** group SH, **c** group SSS, and **d** group SSW

[30, 32] observed that increasing the alkali dosage, leads to an increase of reaction extent and thus to a stronger material. However, there is an optimum content, as high amount of alkalis induce free alkalis in the structure which can then lead to efflorescence [66]. For metakaolin geopolymers this threshold is determined by the molar ratio Na_2O/Al_2O_3 [67], which in this study it's determined to be in the range of 0.97 to 1.03.

In Fig. 6c, the effect of the sodium silicate solution (varying both sodium silicate and water content) is presented, and it can be observed that the metakaolin geopolymer paste (SSS1) has the highest compressive strength (44.1 MPa) at 28 days, having a molar ratio of Na_2O/Al_2O_3 at 0.97, a molar ratio of SiO_2/Al_2O_3 at 3.14 and a water-to-solids ratio of 0.51. This also corresponds to the paste with the lowest drying shrinkage, lower concentration of macropores, and thus greater volume stability.

Finally, in Fig. 6d it can be seen that the increase of solid sodium silicate maintaining water/solids constant to 0.51, seems to improve the compressive strength (SSW2) up to

a certain degree, beyond which higher content of solid sodium silicate seems to detriment the strength (SSW3). This strength reduction was not expected as previous literature observe strength enhancement up to SiO_2/Al_2O_3 ratios of 3.5 [27], but Zhang [30] and Albidah [34] have reported this strength reduction when the molar ratio SiO_2/Al_2O_3 is increased as a result of the impedance of geopolymerization caused by Al–Si precipitation in which the excess silicate inhibits the water evaporation and structure formation. This was also supported by its higher drying shrinkage and mass loss in Sect. 3.3.

Thereafter, the strength development gained at 28 days by all the different metakaolin geopolymer pastes has been compared to the standard EN strength class of 32.5 MPa required at 28 days [68]. The specimens with water-to-solids ratio > 0.52, or with a molar ratio $Na_2O/Al_2O_3 > 1.03$ seem to develop lower compressive strengths than the required by the standard. The strengths obtained in this study are within the range of prior studies [27, 28, 33], which suggested that the optimal molar oxide ratios

for metakaolin geopolymer pastes are water-to-solids ≈ 0.5, $Na_2O/Al_2O_3 = 0.6–1$ and $SiO_2/Al_2O_3 ≈ 3$.

It has to be noted that besides the molar oxide ratios, the curing conditions of the pastes (temperature, relative humidity) have also a great influence on the strength development of metakaolin geopolymers [69]. For similar oxide ratios to the ones in this study, strengths above 50 MPa have been reported when curing at temperatures above 40 °C for the first hours [70, 71].

3.5 Thermal analysis (TGA/DSC)

The TGA–DSC analysis was performed for all the geopolymer formulations to investigate their thermal stability at 7 and 28 days. In Fig. 7, the TGA–DSC curve of a 28 day cured reference geopolymer (REF) is shown. The first observation is that there is a pronounced mass loss of 16% below 200 °C in the TGA curve. This mass loss of the metakaolin geopolymer is probably due to the loss of weakly bound water. This is in agreement with the literature that associates this mass loss with the loss of remaining free water and slightly bound water in the geopolymer structure [72, 73]. Accordingly, two endothermic peaks are visible in the DSC curve. From 200 to 600 °C, a further 3% mass loss is observed and is associated with the loss of bound water generated by the polymerization reaction of silanol and aluminol group (Si–OH and Al–OH) on the surface gels (dehydration of N–A–S–H gel) [59, 73].

Other studies [74, 75], observed a further mass loss around 600–700 °C and that is due to the presence of unreacted kaolin in the metakaolin. However, that was not observed in this study.

The TGA–DSC curves of all the geopolymer mixes had similar behaviour to the REF geopolymer curves shown in Fig. 7. All of them presented most of their mass loss below 200 °C, having a total mass loss varying from 15 to 20% at 600 °C. This total mass loss is lower than for cement pastes, which can reach 30% mass loss at 600 °C having a water/cement ratio of 0.33 [76]. In most of the samples, there was also a slight decrease of mass loss observed between 7 and 28 days of curing (between 0.3 and 1%) due to the progress of the geopolymerization [77]. However, a more markedly change was observed when varying the NaOH concentration. Figure 8 illustrates the TGA curves of the mixes SH1, SH2 and SH3 at curing ages of 7 and 28 days. From the curves it can be seen that there is a total higher mass loss at higher contents of NaOH (SH1 > SH2 > SH3). This mass loss could be mainly attributed to two different factors: (i) due to its hygroscopic nature, if there are free alkalis in the macropores they might be absorbing water during curation at 80% relative humidity, leading to a higher water evaporation and (ii) higher content of NaOH could be leading to higher bound water to the geopolymer structure that is then dihydroxilated between 200 and 600 °C (Fig. 8) [72, 78].
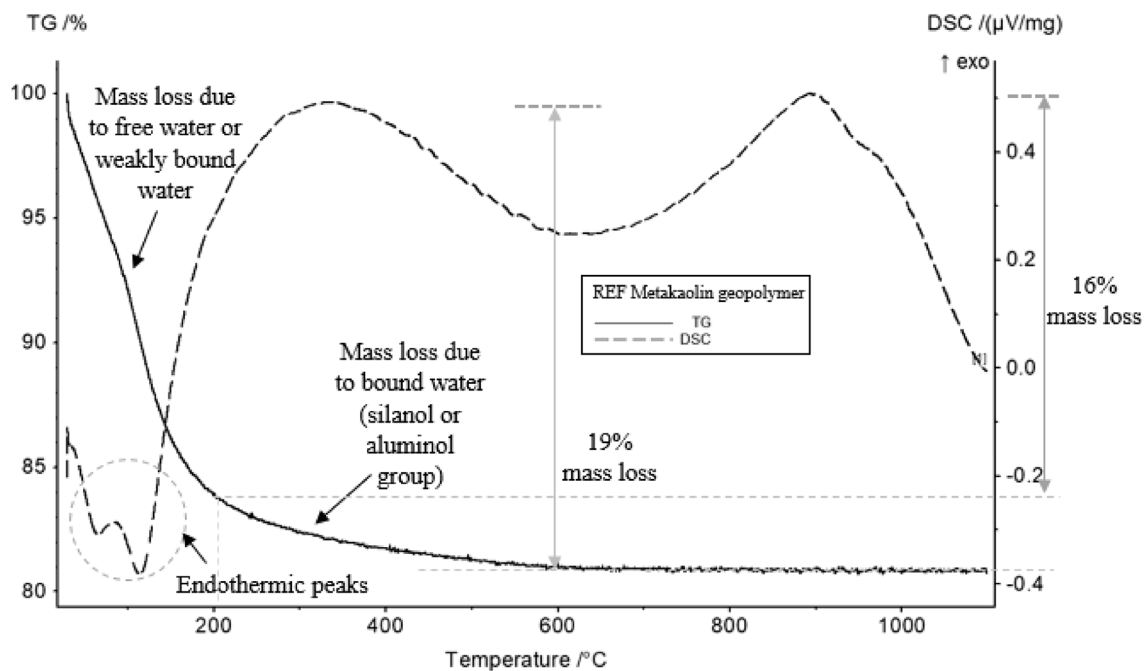

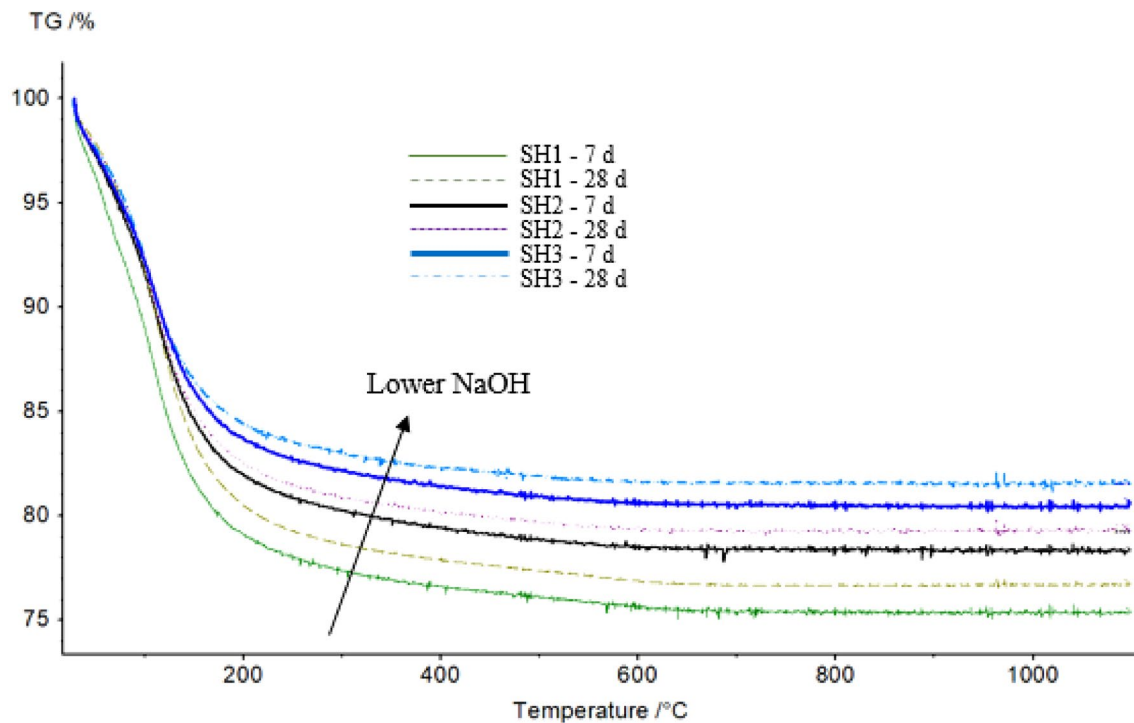**Fig. 7** TGA–DSC curve of REF metakaolin geopolymer

Fig. 8 TGA curves of SH1, SH2 and SH3 at 7 and 28 days

3.6 SEM–EDS analysis

Figure 9 shows four secondary electron images of 28 day aged samples, one from each group (W3, SH1, SSS1, SSW2) with a ×500 magnification. The main observations are that the sample with an increased water content (W3) presents the largest visible macropores, whereas the sample with the highest amount of sodium hydroxide (SH1) presents the most visible cracks in its microstructure. This correlates with the fact that W3 had the highest mass loss, and this is probably due to an increased porosity that tends to weaken the overall structure, lowers the sample's weight and overall strength. Similarly, SH1 led to the highest drying shrinkage, and generally, the drying shrinkage that occurs during the densification of the gel results in the formation of cracks and decrease of strength [65], which was also corroborated by the lower strength observed in Sect. 3.4. Samples SSW2 and SSS1, show a more dense microstructure, with less voids, and less cracks, when compared to W3 and SH1. This also correlates with their corresponding strength, SSW2 and SSS1, reached compressive strengths of 34.7 MPa and 44.1 MPa after 28 days respectively, while W3 and SH1 lead to 23.8 MPa and 26.5 MPa, respectively. The SEM micrographs of Fig. 9 were also screened by EDS to identify the different phases present in the surface. This analysis identified partially reacted metakaolin particles (greyish colour) embedded

in the geopolymer binder phase (background grey), some undissolved particles which were mainly titanium and iron based (bright whitish colour), and the most dark areas of the surface were identified as pores [65]. Moreover, all samples presented some fractured lines which were related to cracks, probably originated during drying shrinkage.

3.7 XRD analysis

Figure 10 shows the XRD diffractograms of the different group samples when compared to the precursor metakaolin. From the figure, it can be seen that the metakaolin diffractogram has a characteristic broad peak centred at 22° 2θ. This peak is often referred in the literature as hump or halo peak, and it indicates the presence of an amorphous phase. It can also be seen that all the metakaolin-based geopolymers present this amorphous hump between 15 to 40° 2θ. The literature [73] relates this broad peak to the formation of N–A–S–H gel, and the size of it depends on the amount of gel produced. It has also been observed that in metakaolin geopolymers those broad peaks are shifted to higher 2θ angles. This indicates that there has been a dissolution of the amorphous phase present in the raw material, and a new amorphous phase has originated. Another observation from the XRD patterns is that the displacement to higher
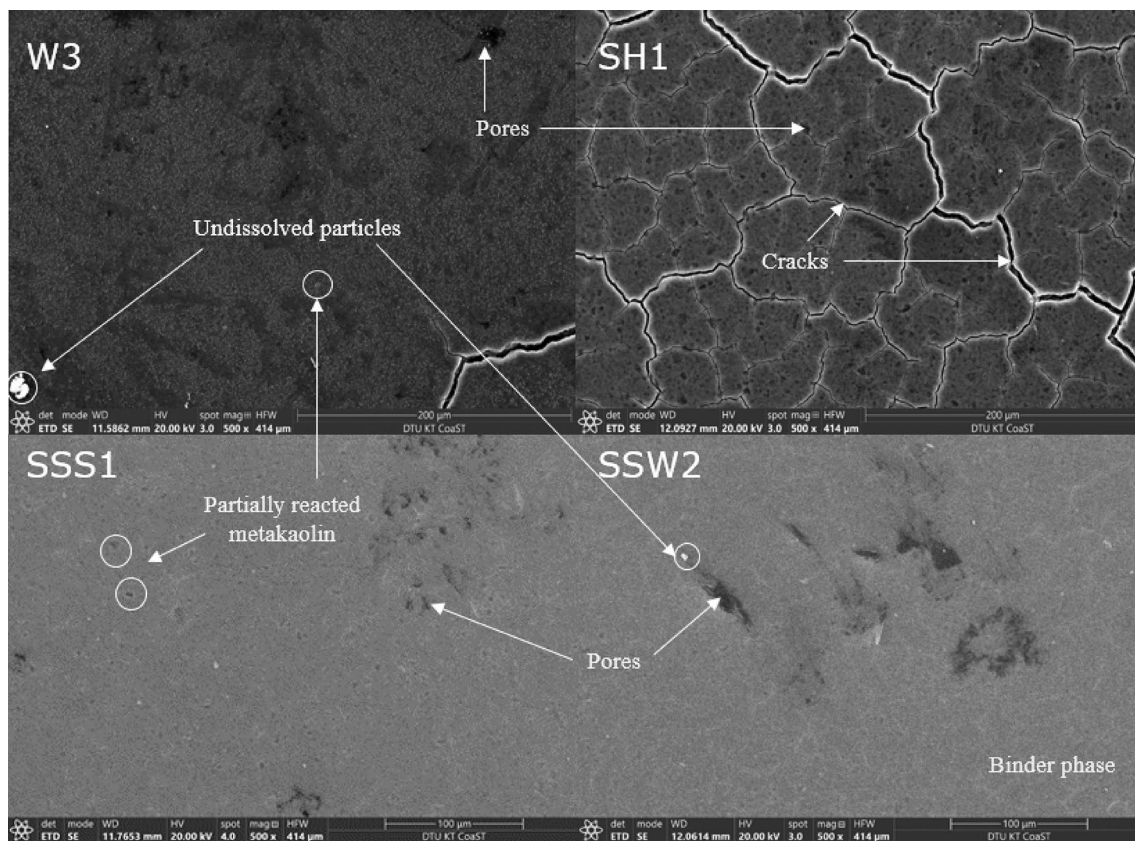
Fig. 9 SEM images of 28 day cured samples (W3, SH1, SSS1, SSW2) with varying content of water and sodium hydroxide measured at 20 kV and × 500

2θ angles tends to be larger for the samples with water-to-solids between 0.51 and 0.52 of each sample group.

Both in the metakaolin and in the synthesized geopolymers, the main crystalline phases that have been detected are quartz (PDF #46-1045) and anatase (PDF #21-1272). This indicates that the crystals do not dissolve in the alkaline activator solution and therefore do not intervene in the geopolymerization, but rather stay in the form of inactive charges in the geopolymer [77]. Not many differences have been detected among the XRD patterns of the metakaolin geopolymers produced, except for W1, in which it has also been identified muscovite (PDF #07-0042) at 30 2θ°, this could have been associated with an increased water content with respect to REF, however, it has not been detected in W2 nor W3. Thus, it could just be associated to a residual crystalline impurity.

4 Conclusions

This study investigated 13 mix formulations of metakaolin geopolymers to understand better the effect of the water, NaOH and Na_2SiO_3 content on fresh and hardened properties.

- An increase of the water-to-solids ratio above 0.52 has been shown to increase the fluidity and reduce the viscosity of the fresh pastes, but in the meantime it has led to higher porosity and mass loss during the hardening evolution, and consequently lower compressive strength development. It was also noted that pastes with water-to-solids ratio below 0.49 were not workable enough to proceed with experiments.
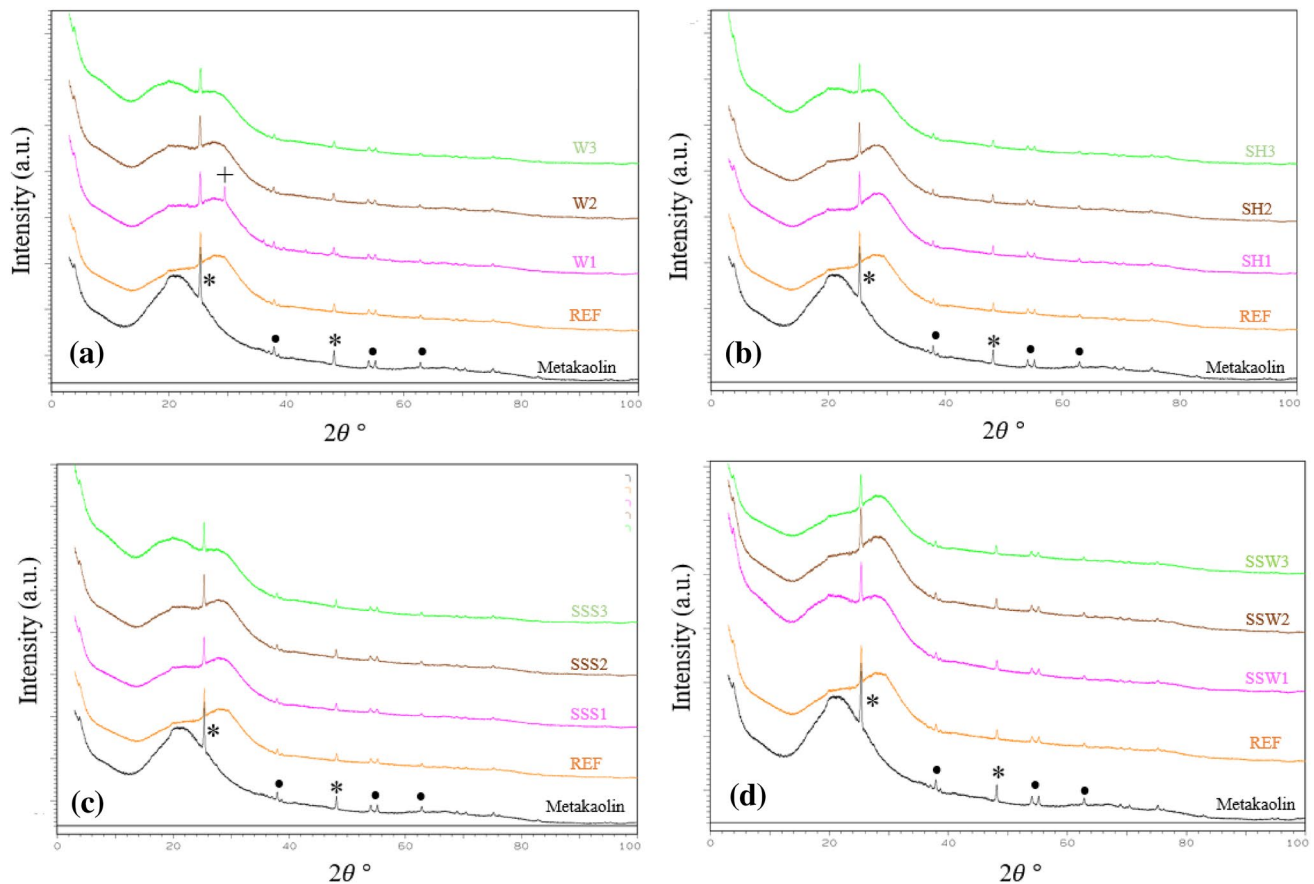
Fig. 10 XRD of raw Metakaolin compared to **a** group W, **b** group SH, **c** group SSS, and **d** group SSW. Identified phases are quartz (∗), anatase (.), and muscovite (+)

- The optimal content of NaOH is tightly influenced by the Na_2O/Al_2O_3 ratio. The optimum values found in this study are in the range of 0.97–1.03. Lower values than this range were seen to mainly affect the strength development of the pastes, not being able to reach the minimum requirement of 32.5 MPa after 28 days. Conversely, higher values seemed to affect negatively the fluidity of the paste, accelerating the setting time, increasing the shrinkage and cracking during hardening and ultimately not favouring the long-term strength development.

- The Na_2SiO_3 solution was added as a secondary source of soluble silica, and its optimal content is greatly affected by the SiO_2/Al_2O_3 and water-to-solids ratio. The optimal combination was found in paste SSS1 which had a $SiO_2/Al_2O_3 = 3.14$ and a water/solids = 0.51, and led to the highest compressive strength (44.1 MPa) after 28 days.

In addition, the SEM–EDS analysis corroborated the mass loss, shrinkage and strength results, while TGA–DSC and XRD presented the progress of the reaction and identified the presence of N–A–S–H phase in the pastes.

Overall, metakaolin geopolymers can lead to compressive strengths above 32.5 MPa when having appropriate mix designs that balance the water, alkali and silica content to not be in deficit or surplus, but in the right proportion, enhancing the overall performance. In this study, the optimal proportions were found to be SiO_2/Al_2O_3 at 3.14, Na_2O/Al_2O_3 at 0.97 and water-to-solids ratio of 0.51. Nevertheless, it would be recommended to investigate further how to improve the workability of the pastes, maybe by the addition of superplasticizers to reduce the water demand. It would also be encouraged to test other curing conditions that could be used in the pre-cast industry, and evaluating the durability of those pastes at different environmental conditions.

PAJ: writing-review & editing, visualization. AJD: writing-review & editing, visualization. NR: conceptualization, writing-review & editing, visualization. LSJ: writing- review & editing, visualization. MC: writing-review & editing, visualization.

Declarations

Conflict of interest The authors declare that they have no known competing financial interests or personal relationships that could have appeared to influence the work reported in this paper.

Ethical approval This article does not contain any studies with human participants or animals performed by any of the authors.

References

1. Pavithra P et al (2016) A mix design procedure for geopolymer concrete with fly ash. J Clean Prod 133:117–125
2. Farfan J, Fasihi M, Breyer C (2019) Trends in the global cement industry and opportunities for long-term sustainable CCU potential for power-to-X. J Clean Prod 217:821–835
3. Birol F (2020) Energy technology perspectives. International Energy Agency, Paris
4. McLellan BC, Williams RP, Lay J, Van Riessen A, Corder GD (2011) Costs and carbon emissions for geopolymer pastes in comparison to ordinary portland cement. J Clean Prod 19(9–10):1080–1090
5. Luukkonen T, Abdollahnejad Z, Yliniemi J, Kinnunen P, Illikainen M (2018) One-part alkali-activated materials: a review. Cem Concr Res 103:21–34
6. Van Deventer JS, Provis JL, Duxson P (2012) Technical and commercial progress in the adoption of geopolymer cement. Miner Eng 29:89–104
7. Maddalena R, Roberts JJ, Hamilton A (2018) Can Portland cement be replaced by low-carbon alternative materials? A study on the thermal properties and carbon emissions of innovative cements. J Clean Prod 186:933–942
8. Torres-Carrasco M, Puertas F (2017) Alkaline activation of aluminosilicates as an alternative to Portland cement: a review. Rev Rom Mater 47(1):3–15
9. Provis JL, Bernal SA (2014) Geopolymers and related alkali-activated materials. Annu Rev Mater Res 44:299–327
10. Khale D, Chaudhary R (2007) Mechanism of geopolymerization and factors influencing its development: a review. J Mater Sci 42(3):729–746
11. El Hafid K, Hajjaji M, El Hafid H (2017) Influence of NaOH concentration on microstructure and properties of cured alkali-activated calcined clay. J Build Eng 11:158–165
12. Provis JL, Van Deventer JSJ (eds) (2009) Geopolymers: structures, processing, properties and industrial applications. Elsevier, Amsterdam, pp 1–66
13. Ito A, Wagai R (2017) Global distribution of clay-size minerals on land surface for biogeochemical and climatological studies. Sci Data 4(1):1–11
14. Abdullah MM, Ming LY, Yong HC, Tahir MF (2018) Clay-based materials in geopolymer technology. Cement based material, 1st edn. IntechOpen, London, p 239
15. Mustafa Al Bakri AM et al (2012) Effect of Na_2SiO_3/NaOH ratios and NaOH molarities on compressive strength of fly-ash-based geopolymer. ACI Mater J 109:1–14
16. Provis JL (2018) Alkali-activated materials. Cem Concr Res 114:40–48
17. Arbi K, Nedeljkovic M, Zuo Y, Ye G (2016) A review on the durability of alkali-activated fly ash/slag systems: advances, issues, and perspectives. Ind Eng Chem Res 55(19):5439–5453
18. Li N, Shi C, Zhang Z, Wang H, Liu Y (2019) A review on mixture design methods for geopolymer concrete. Composites B 178:107490
19. Wattimena OK, Antoni A, Hardjito D (2017) A review on the effect of fly ash characteristics and their variations on the synthesis of fly ash based geopolymer. AIP Conf Proc 1887(1):020041
20. Naghizadeh A, Ekolu SO (2019) Method for comprehensive mix design of fly ash geopolymer mortars. Constr Build Mater 202:704–717
21. Ferdous MW, Kayali O, Khennane A (2013) A detailed procedure of mix design for fly ash based geopolymer concrete. In: Proceedings of the fourth Asia-Pacific conference on FRP in structures (APFIS 2013), Melbourne, Australia pp 11–13
22. Xu Z, Yue J, Pang G, Li R, Zhang P, Xu S (2021) Influence of the activator concentration and solid/liquid ratio on the strength and shrinkage characteristics of alkali-activated slag geopolymer pastes. Adv Civil Eng 2021:1–11
23. Humad AM, Provis JL, Habermehl-Cwirzen K, Rajczakowska M, Cwirzen A (2021) Creep and long-term properties of alkali-activated Swedish-slag concrete. J Mater Civil Eng. https://doi.org/10.1061/(ASCE)MT.1943-5533.0003381
24. Serag Faried A, Sofi WH, Taha AZ, El-Yamani MA, Tawfik TA (2020) Mix design proposed for geopolymer concrete mixtures based on ground granulated blast furnace slag. Aust J Civ Eng 18(2):205–218
25. Provis JL, Duxson P, van Deventer JS (2010) The role of particle technology in developing sustainable construction materials. Adv Powder Technol 21(1):2–7
26. Shi C, Qu B, Provis JL (2019) Recent progress in low-carbon binders. Cem Concr Res 122:227–250
27. Liew YM, Heah CY, Kamarudin H (2016) Structure and properties of clay-based geopolymer cements: a review. Prog Mater Sci 83:595–629
28. Duxson P, Provis JL, Lukey GC, Mallicoat SW, Kriven WM, Van Deventer JS (2005) Understanding the relationship between geopolymer composition, microstructure and mechanical properties. Colloids Surf A 269(1–3):47–58

29. Juengsuwattananon K, Winnefeld F, Chindaprasirt P, Pimraksa K (2019) Correlation between initial SiO_2/Al_2O_3, Na_2O/Al_2O_3, Na_2O/SiO_2 and H_2O/Na_2O ratios on phase and microstructure of reaction products of metakaolin-rice husk ash geopolymer. Constr Build Mater 226:406–417

30. Wang J, Zhang C, Xu J, Qu P, Zhou Y, Han HM (2012) The effect of alkali on compressive of metakaolin based geopolymeric cement. Adv Mater Res 554:327–330

31. Kuenzel C, Neville TP, Donatello S, Vandeperre L, Boccaccini AR, Cheeseman CR (2013) Influence of metakaolin characteristics on the mechanical properties of geopolymers. Appl Clay Sci 83:308–314

32. Longhi MA, Rodriguez ED, Walkley B, Zhang Z, Kirchheim AP (2020) Metakaolin-based geopolymers: relation between formulation, physicochemical properties and efflorescence formation. Composites B 182:107671

33. Chen L, Wang Z, Wang Y, Feng J (2016) Preparation and properties of alkali activated metakaolin-based geopolymer. Materials 9(9):767

34. Albidah A, Alghannam M, Abbas H, Almusallam T, Al-Salloum Y (2021) Characteristics of metakaolin-based geopolymer concrete for different mix design parameters. J Market Res 10:84–98

35. Alghannam M, Albidah A, Abbas H, Al-Salloum Y (2021) Influence of critical parameters of mix proportions on properties of MK-based geopolymer concrete. Arab J Sci Eng 46(5):4399–4408

36. Lee S, Kim B, Seo J, Cho S (2020) Beneficial use of MIBC in metakaolin-based geopolymers to improve flowability and compressive strength. Materials 13(17):3663

37. CEN: European Committee for Standardization (2005) EN 196-3: methods of testing cement part 3—determination of setting times and soundness

38. Ranjbar N, Mehrali M, Kuenzel C, Gundlach C, Pedersen DB, Dolatshahi-Pirouz A, Spangenberg J (2021) Rheological characterization of 3D printable geopolymers. Cem Concr Res 147:106498

39. de Gasperi J, Holthusen D, Howes MFD, Sattler N, Longhi MA, Rodríguez ED (2021) Temporal dynamics of rheological properties of metakaolin-based geopolymers: effects of synthesis parameters. Constr Build Mater 289:123145

40. Poulesquen A, Frizon F, Lambertin D (2011) Rheological behavior of alkali-activated metakaolin during geopolymerization. J Non-Cryst Solids 357(21):3565–3571

41. Bao K, Lavrov A, Nilsen HM (2016) Numerical modelling of non-newtonian fluid flow in fractures and porous media. In ECMOR XV-15th European conference on the mathematics of oil recovery. European Association of Geoscientists & Engineers pp cp-494

42. Sant G, Ferraris CF, Weiss J (2008) Rheological properties of cement pastes: a discussion of structure formation and mechanical property development. Cem Concr Res 38(11):1286–1296

43. Struble L, Sun GK (1995) Viscosity of Portland cement paste as a function of concentration. Adv Cem Based Mater 2(2):62–69

44. Skripkiunas G, Karpova E, Bendoraitiene J, Barauskas I (2020) Rheological properties and flow behaviour of cement-based materials modified by carbon nanotubes and plasticising admixtures. Fluids 5(4):169

45. De La Rosa Á, Ruiz G, Castillo E, Moreno R (2021) Calculation of dynamic viscosity in concentrated cementitious suspensions: probabilistic approximation and Bayesian analysis. Materials 14(8):1971

46. Favier A, Hot J, Habert G, Roussel N, de Lacaillerie JBDE (2014) Flow properties of MK-based geopolymer pastes. A comparative study with standard Portland cement pastes. Soft Matter 10(8):1134–1141

47. Rifaai Y, Yahia A, Mostafa A, Aggoun S, Kadri EH (2019) Rheology of fly ash-based geopolymer: effect of NaOH concentration. Constr Build Mater 223:583–594

48. Siyal AA, Azizli KA, Man Z, Ullah H (2016) Effects of parameters on the setting time of fly ash based geopolymers using Taguchi method. Procedia Eng 148:302–307

49. Abdul Rahim RH, Mohd Azizli KA, Rahmiati T, Nuruddin F (2014) Effect of sodium hydroxide concentration on the mechanical property of nonsodium silicate fly ash based geopolymer. J Appl Sci 14:3381–3384

50. Malkawi AB, Nuruddin MF, Fauzi A, Almattarneh H, Mohammed BS (2016) Effects of alkaline solution on properties of the HCFA geopolymer mortars. Procedia Eng 148:710–717

51. Kubba Z, Hewayde E, Huseien GF, Sam ARM, Asaad MA (2019) Effect of sodium silicate content on setting time and mechanical properties of multi blend geopolymer mortars. J Eng Appl Sci 14:2262–2267

52. Si R, Dai Q, Guo S, Wang J (2020) Mechanical property, nanopore structure and drying shrinkage of metakaolin-based geopolymer with waste glass powder. J Clean Prod 242:118502

53. Ling Y, Wang K, Fu C (2019) Shrinkage behavior of fly ash based geopolymer pastes with and without shrinkage reducing admixture. Cement Concr Compos 98:74–82

54. Yang T, Zhu H, Zhang Z (2017) Influence of fly ash on the pore structure and shrinkage characteristics of metakaolin-based geopolymer pastes and mortars. Constr Build Mater 153:284–293

55. Kuenzel C, Vandeperre LJ, Donatello S, Boccaccini AR, Cheeseman C (2012) Ambient temperature drying shrinkage and cracking in metakaolin-based geopolymers. J Am Ceram Soc 95(10):3270–3277

56. Park S, Yu J, Oh JE, Pyo S (2022) Effect of silica fume on the volume expansion of metakaolin-based geopolymer considering the silicon-to-aluminum molar ratio. Int J Concrete Struct Mater 16(1):1–12

57. Li Z, Gao P, Ye G (2017) Experimental study on autogenous deformation of metakaolin based geopolymer. In 2nd Int. RILEM/COST Conf. Early Age Crack. Serv. Cem. Mater. Struct., Brussels pp 209–214

58. Wang H, Li H, Yan F (2005) Synthesis and mechanical properties of metakaolinite-based geopolymer. Colloids Surf A 268(1–3):1–6

59. Skripkiūnas G, Sasnauskas V, Daukšys M, Palubinskaite D (2007) Peculiarities of hydration of cement paste with addition of hydrosodalite. Mater Sci-Pol 25(3):632–634

60. Kamang EJ, Oyemogum IM, & Ndanusa FW (2013) Volcanic ash, metakaolin and ordinary portland cement blends in concrete production. Central Europe Toward Sustainable Building (CESB13)

61. Hasnaoui A, Ghorbel E, Wardeh G (2019) Comparison between Portland cement concrete and geopolymer concrete based on metakaolin and granulated blast furnace slag with the same binder volume. Acad J Civil Eng 37(2):127–132

62. Wong HHC, Kwan AK (2008) Packing density of cementitious materials: measurement and modelling. Mag Concr Res 60(3):165–175

63. Abideng HAWA, Tonnayopas D, Prachasaree W (2014) Performance evaluation of metakaolin based geopolymer containing parawood ash and oil palm ash blends. Mater Sci 20(3):339–344

64. Davidovits J (1994) Geopolymers: man-made rock geosynthesis and the resulting development of very early high strength cement. J Mater Educ 16:91–91

65. Burciaga-Diaz O, Escalante-Garcia JI, Magallanes-Rivera RX (2015) Compressive strength and microstructural evolution of

metakaolin geopolymers exposed at high temperature. ALCO-PAT J 5(1):52–66

66. Longhi MA, Zhang Z, Walkley B, Rodríguez ED, Kirchheim AP (2021) Strategies for control and mitigation of efflorescence in metakaolin-based geopolymers. Cem Concr Res 144:106431

67. Latella BA, Perera DS, Durce D, Mehrtens EG, Davis J (2008) Mechanical properties of metakaolin-based geopolymers with molar ratios of Si/Al ≈ 2 and Na/Al ≈ 1. J Mater Sci 43(8):2693–2699

68. Sanjuán MA, Argiz C (2012) The new European standard on common cements specifications EN 197–1: 2011. Mater Constr 62(307):425–430

69. Garcí TA, de Lourdes Chávez-Garcí M (2016) Compressive strength of metakaolin-based geopolymers: influence of KOH concentration, temperature, time and relative humidity. Mater Sci Appl 7(11):772–791

70. Mo BH, Zhu H, Cui XM, He Y, Gong SY (2014) Effect of curing temperature on geopolymerization of metakaolin-based geopolymers. Appl Clay Sci 99:144–148

71. Castillo H, Collado H, Droguett T, Sánchez S, Vesely M, Garrido P, Palma S (2021) Factors affecting the compressive strength of geopolymers: a review. Minerals 11(12):1317

72. Tchakouté HK, Rüscher CH, Kong S, Kamseu E, Leonelli C (2017) Thermal behavior of metakaolin-based geopolymer cements using sodium waterglass from rice husk ash and waste glass as alternative activators. Waste Biomass Valor 8(3):573–584

73. Chen K, Lin WT, Liu W (2021) Effect of NaOH concentration on properties and microstructure of a novel reactive ultra-fine fly ash geopolymer. Adv Powder Technol 8:2933–2936

74. Caballero LR, Paiva MDDM, Fairbairn EDMR, Toledo RD (2019) Thermal, mechanical and microstructural analysis of metakaolin based geopolymers. Mater Res. https://doi.org/10.1590/1980-5373-mr-2018-0716

75. MejíadeGutiérrez R, Torres AJ, Guerrero CE (2004) Analysis of thermal process of pozzolan production. Mater Constr 54(274):65–72. https://doi.org/10.3989/mc.2004.v54.i274.233

76. Alarcon-Ruiz L, Platret G, Massieu E, Ehrlacher A (2005) The use of thermal analysis in assessing the effect of temperature on a cement paste. Cem Concr Res 35(3):609–613

77. Douiri H, Louati S, Baklouti S, Arous M, Fakhfakh Z (2016) Enhanced dielectric performance of metakaolin–H_3PO_4 geopolymers. Mater Lett 164:299–302

78. Kioupis D, Skaropoulou A, Tsivilis S, Kakali G (2018) Alkali leaching control of construction and demolition waste based geopolymers. MATEC Web Conf 149:01064

Publisher's Note Springer Nature remains neutral with regard to jurisdictional claims in published maps and institutional affiliations.